Time-Resolved O_3 Chemical Chain Reaction Kinetics via High-Resolution IR Laser Absorption Methods

Axel Kulcke,† Brad Blackmon, William B. Chapman, In Koo Kim, and David J. Nesbitt*

JILA, National Institute of Standards and Technology and University of Colorado, and Department of Chemistry and Biochemistry, University of Colorado, Boulder, Colorado 80309-0440

Received: July 29, 1997; In Final Form: December 9, 1997

Excimer laser photolysis in combination with time-resolved IR laser absorption detection of OH radicals has been used to study O_3/OH($v = 0$)/HO_2 chain reaction kinetics at 298 K, (i.e., $OH + O_3 \xrightarrow{k_1} HO_2 + O_2$ and $HO_2 + O_3 \xrightarrow{k_2} OH + 2O_2$). From time-resolved detection of OH radicals with high-resolution near IR laser absorption methods, the chain induction kinetics have been measured at up to an order of magnitude higher ozone concentrations ($[O_3] \leq 10^{17}$ molecules/cm^3) than accessible in previous studies. This greater dynamic range permits the full evolution of the chain induction, propagation, and termination process to be temporally isolated and measured in real time. An exact solution for time-dependent OH evolution under pseudo- first-order chain reaction conditions is presented, which correctly predicts new kinetic signatures not included in previous OH + O_3 kinetic analyses. Specifically, the solutions predict an initial exponential loss (chain "induction") of the OH radical to a steady-state level ($[OH]_{ss}$), with this fast initial decay determined by the *sum* of both chain rate constants, $k_{ind} = k_1 + k_2$. By monitoring the chain induction feature, this sum of the rate constants is determined to be $k_{ind} = 8.4(8) \times 10^{-14}$ cm^3 molecule^{-1} s^{-1} for room temperature reagents. This is significantly higher than the values currently recommended for use in atmospheric models, but in excellent agreement with previous results from Ravishankara et al. [*J. Chem. Phys.* **1979**, *70*, 984].

I. Introduction

The chemistry of the middle and upper atmosphere reflects an intricate hierarchy of energy transfer, reaction dynamics, and bulk transport phenomena for both homogeneous and heterogeneous phases.[1,2] One focus of kinetic measurements has been toward the chemistry of ozone chain reactions,[3−12] which play a crucially important role in the photochemistry of the atmosphere. There has been much effort elucidating ozone depletion kinetics in the polar regions due to chlorine radical processes in high-altitude stratospheric clouds.[13−16] However, of particular interest in the midlatitudes has been the catalytic odd hydrogen ozone cycle[17]

$$OH + O_3 \xrightarrow{k_1} HO_2 + O_2 \quad (1)$$

$$HO_2 + O_3 \xrightarrow{k_2} OH + 2O_2 \quad (2)$$

that is predicted from modeling studies[18−20] to be important in determining ozone height profiles. One of the distinguishing features of this chain reaction is that it does not involve free oxygen atoms, which therefore makes it kinetically viable in the lower stratosphere/upper troposphere where the O atom concentrations are constrained by three body recombination with O_2. This kinetic importance at lower elevations has spurred interest in potential anthropogenic effects on these chain processes, in particular due to the enhanced loading[3] of NO_x and H_2O vapor from supersonic traffic in the 10−20 km region. Additional focus on the OH and HO_2 radical chain cycles stems from their relevance in oxidation pathways throughout the troposphere. For example, HO_2 is strongly interlinked with OH not only through the ozone chain reaction described above but also by reaction with NO_x species,

$$HO_2 + NO \rightarrow OH + NO_2 \quad (3)$$

whose concentrations can be significantly perturbed by aircraft emissions. As a result, there has been keen interest in obtaining reliable rate constant data for these OH/HO_2 chain processes in order to facilitate accurate models of the relevant atmospheric phenomena.

Due to the atmospheric importance of such OH/HO_2 chain rates, there have been several studies of reactions 1 and 2 based on laser induced fluorescence (LIF), resonance fluorescence (RF), and laser magnetic resonance (LMR) detection schemes.[4−9] Rates for the HO_2 + O_3 chain reaction step have proven especially challenging to obtain directly with conventional discharge flow/LIF methods due to kinetic competition with the faster OH + O_3 chain step. Clever $^{16}O/^{18}O$ isotopic substitution methods by Zahniser and Howard[6] and Sinha et al.[9] have been used in conjunction with laser magnetic resonance (LMR) studies to circumvent these problems, yielding k_2 values in the temperature regime above 243 K. However, the resulting Arrhenius plots are significantly curved, which complicates extrapolation to much lower temperatures. The effects of kinetic competition on measurements of the faster OH + O_3 chain step are much less severe; k_1 has therefore been studied by monitoring the time and/or distance dependence of [OH] based on electronic excitation of the $A(^2\Sigma)-X(^2\Pi)$ band with LIF/RF flow cell methods.[4,5,7] The reported rate constants for k_1 cover a surprisingly wide range, varying by as much as 30−50% (from 5.5−8.2) $\times 10^{-14}$ cm^3 molecule^{-1} s^{-1}) under room

† Optima Handels GMBH, Austria.

S1089-5639(97)02486-9 CCC: $15.00
Published on Web 02/24/1998

TABLE 1: Rate Constants for $OH/HO_2/O_3$ Chain Reaction Kinetics

k_{ind} (cm^3 $molecule^{-1}$ s^{-1})	source
$5.5(15) \times 10^{-14}$ [a]	Anderson and Kaufman (ref 4)
$6.5(10) \times 10^{-14}$ [a]	Kurylo (ref 5)
8.2×10^{-14} [a]	Ravishankara et al. (ref 7)
$6.5(10) \times 10^{-14}$ [b]	Zahniser and Howard (ref 6)
$7.46(16) \times 10^{-14}$	Smith et al. (ref 8)
6.8×10^{-14} [c]	JPL recommended value (ref 1)
$8.4(8) \times 10^{-14}$	this work

[a] The values are based on an approximate analysis that neglects chain reaction effects; the reported rates more appropriately represent k_{ind} (see text). [b] The results of Zahniser and Howard use ^{18}O isotopic labeling to isolate the two chain reaction steps, and therefore represent k_1 rather $k_1 + k_2$. [c] The JPL recommendation represents an average over several literature values.

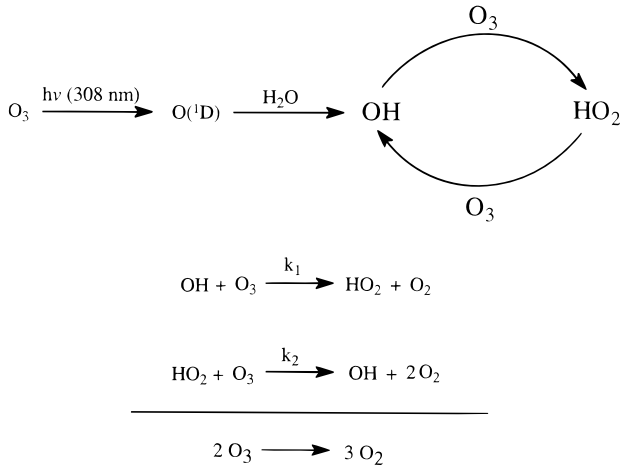

Figure 1. Reaction scheme for the investigated reactions including the atmospheric relevant ozone depleting chain reaction.

temperature conditions (see Table 1). The currently recommended value for use in atmospheric modeling reflects an average over this wide distribution of rate measurements.

The fundamental importance of these atmospheric processes has motivated us to develop alternate methods for study of fast radical chain reaction kinetics.[21−23] Specifically, we have developed an approach based on direct absorption spectroscopy with high-resolution IR lasers, which permits the absolute OH radical density to be probed directly in real time.[24,25] Most importantly, the use of a near IR instead of UV probe allows much higher concentrations of ozone, which provides access to an entirely different regime for study of chemical chain reaction kinetics. The focus of the present work is to describe and apply these high-resolution flash kinetic methods to an investigation of the $O_3/OH/HO_2$ chemical chain reaction system under room temperature conditions. Extension of these measurements down to temperatures (<200 K) relevant to stratospheric modeling is currently underway.

The method is indicated schematically in Figure 1 and can be summarized as follows. Pulsed UV excitation with a XeCl excimer laser is used to generate $O(^1D)$ radicals via weak photolysis of O_3 at 308 nm, which rapidly react with H_2O and are equilibrated by buffer gas collisions to form rovibrationally relaxed OH radicals at the flow cell temperature on a few microsecond time scale. Even for the highest O_3 pressures measured in this study, this step is orders of magnitude faster than the subsequent chain reaction; thus, for the purposes of the present kinetic analysis, the photolysis can be considered as essentially instantaneous generation of thermally equilibrated OH radicals. This subsequent evolution of the chain reaction kinetics is then monitored in real time by direct absorption of OH chain radicals via a single mode, color center laser tuned into resonance with a specific spin-orbit and lambda doublet level of the $v_{OH} = 1 \leftarrow 0$ rovibrational manifold.

What makes high-resolution experimental methods advantageous for studying $OH/HO_2/O_3$ chain reactions is several fold. First, the use of high-resolution IR lasers absorption methods allows one to probe the *absolute* quantum state concentrations of OH and HO_2 radicals nonintrusively. This allows us to characterize the rovibrational distribution of radicals in situ, and in particular to ascertain that collisional relaxation of excited OH vibrational levels is complete on the time scale of the chain induction kinetics. This reflects an advantage over laser induced fluorescence (LIF) or resonance fluorescence (RF) probes of OH radicals on the $A(^2\Sigma) \leftarrow X(^2\Pi)$ band, where electronic predissociation[26] occurs rapidly in the upper $A(^2\Sigma)$ state for $v_{OH} > 1$ and/or high rotational levels.

An even more important advantage of probing in the near IR is that ozone, necessarily present in large concentrations, is transparent in the OH stretch region. This is quite different from LIF/RF detection of OH in the 280−300 nm $A(^2\Sigma) \leftarrow X(^2\Pi)$ region, where the Hartley band absorption of ozone is still strong. Furthermore, detection of OH radicals via UV excitation under high O_3 concentration conditions results in secondary photolytic formation of $O(^1D)$, which upon subsequent reaction with H_2O generates additional OH radical chain centers that can complicate the kinetics under investigation. By way of contrast, ozone is nonabsorbing in the 3500 cm^{-1} OH stretch region of the probe laser, which permits the high-resolution near IR methods to study $O_3/OH/HO_2$ chain kinetics at much higher ozone concentrations than previously accessible. These higher ozone concentrations greatly speed up chain propagation kinetics with respect to chain termination processes, which makes it possible to temporally isolate chemical chain reaction kinetics in both the "induction" and steady state "propagation" regime. In light of the appreciable range of rate constant values reported in the literature, an independent room temperature study of these chain rates represents an appropriate first application of these high-resolution near IR methods.

The remainder of this paper is organized as follows. The experimental setup for the high-resolution direct absorption methods is briefly described in section 2. Section 3 presents analytical solutions for the chain reaction kinetics, which are used to extract the rate constant information from the experimental data. The chain reaction rate results are reported in section 4, and compared with previous experimental data. The experimental conclusions and directions for further work are summarized in section 5.

II. Experimental Section

The high-resolution flash kinetic laser apparatus[24,25] is schematically shown in Figure 2. The experiments are based on a combination of (i) flow of initial photolysis precursors and chain reagents in a temperature controlled flow cell, (ii) chain reaction initiation by excimer laser photolysis, and (iii) time-resolved detection of OH chain radicals via IR absorption. The flow tube for the present room temperature kinetic studies is a 97.5 cm Pyrex cylinder of 5 cm diameter and total volume of about 2000 cm^3. The entrance and exit windows to the flow cell are flat CaF_2 plates tilted about 3° from normal incidence to avoid reflections from the surface. The gas outlet of the flow tube is connected via regulating valves to a 16L/s mechanical pump, which allows the pressure and flow rates in the cell to

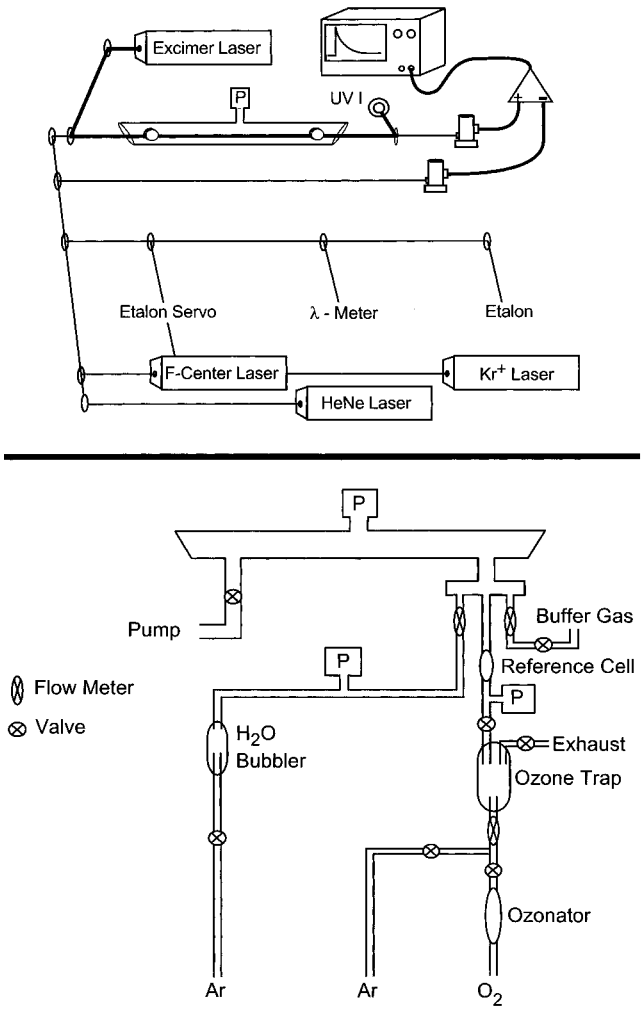

Figure 2. A schematic of the infrared flash kinetic spectrometer and the gas handling system. $O(^1D)$ is produced in the flow tube from 308 nm excimer laser photolysis of O_3 and reacts with H_2O to form OH, which is rapidly relaxed to a thermal distribution by further collisions. The much slower subsequent time dependent evolution of the chain reaction is probed with a single-mode cw color center laser ($\Delta\nu \lesssim 0.0001$ cm^{-1}) tuned to a specific spin orbit and λ-doublet resolved $v = 1 \leftarrow 0$ rovibrational transition in OH. The gas storage and handling system is constructed to control concentrations and flow rates of ozone, water, and buffer gases.

be continuously varied over 3 orders of magnitude. The total pressure in the flow tube is measured at the center of the cell with a capacitance manometer. All inlets/surfaces in the flow cell are made of glass and/or Teflon to minimize decomposition of O_3 on metal surfaces.

Ozone is produced in an AC discharge from molecular oxygen (99.99%) with 2−4% efficiency and adsorbed in a cylinder filled with silica gel at about −110 °C.[27,28] Excess molecular oxygen is removed from the silica gel trap by evacuation at liquid nitrogen temperatures. An adjustable ozone partial pressure in the cell is then maintained by passing a measured flow rate of Ar through the ozone trap at a warmer but fixed temperature. The absolute concentration of O_3 eluted into the Ar flow is determined by absorption of the Hg emission line at 253.7 nm in a calibrated 8.56 mm transmission cell, based on the known absorption cross section[2,29] of $\sigma = 1.137 \times 10^{-17}$ cm^2. A second gas flow into the flow cell is formed by passing a calibrated flow of Ar or SF_6 gas through a porous frit immersed in a H_2O bubbler, which generates a H_2O concentration at the equilibrium vapor pressure. Partial pressures of O_3, H_2O, and Ar buffer gas are determined from knowledge of

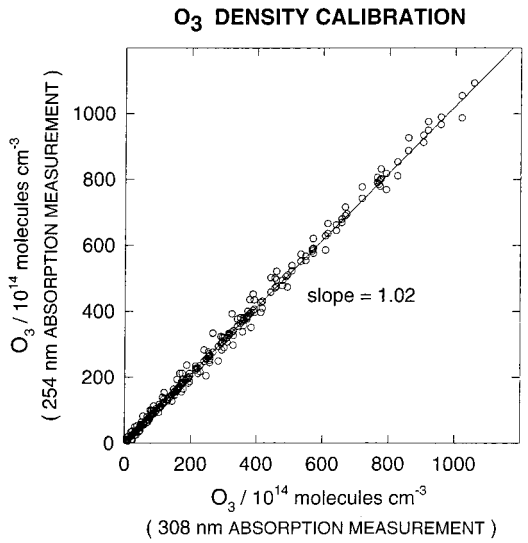

Figure 3. The plot shows the comparison of the ozone concentrations obtained by (i) in situ excimer laser light absorption (308 nm) in the flow cell and (ii) an mercury lamp (254 nm) absorption prior to entrance into the flow cell. The near unity [1.02(4)] slope of this plot indicates quantitative consistency for the 254 nm and 308 nm derived values, with any residual difference within experimental uncertainty. Since a measurement of O_3 concentration in the flow cell is the most direct and avoids any potential issue of decomposition, the $[O_3]$ values used in the kinetic analysis are based on the in situ 308 nm absorption measurement.

partial flow rates and total cell pressure. From these flow meter and calibration measurements, the O_3 reagent concentration in the flow cell can be determined to about ±4%, where the value reflects 2σ uncertainties. Since the ozone concentration measurement can constitute an important source of systematic error in the kinetic analysis, this is also directly tested in situ by 308 nm excimer laser absorption in the flow cell geometry.

The chain reaction is initiated by pulsed photolysis of ozone with an XeCl excimer laser. With unstable resonator optics, the laser emits 10 ns pulses with a rectangular spatial profile of 1 cm × 3 cm, from which the most uniform center of the beam is apertured with a 1 cm^2 iris and directed down the center of the flow cell. The excimer laser is operated at low repetition rates (1−5 Hz), and varied to test for nonlinear kinetic effects due to pulse to pulse accumulation of chain radicals. Pulse energies between 0.1 and 7.5 mJ are selected with neutral density filters. After traversing the flow tube, the UV beam is extracted with a 90° dichroic mirror and steered onto a power meter or pyrolectric detector.

By monitoring the transmitted UV excimer power as a function of gas flow rate, this arrangement conveniently allows the O_3 concentration to be monitored directly in the photolysis cell. For accurate conversion from fractional UV absorption to ozone density, the absorption cross section averaged over the excimer emission profile has to be known reliably. An XeCl Excimer laser with unstable resonator optics has two emission lines at 307.9 and 308.2 nm in an approximately 2:5 integrated intensity ratio.[30] On the basis of known UV absorption spectra,[28,29,31] this translates into an effective absorption cross section for ozone at room temperature of 13.4(5) 10^{-20} cm^2. Thus, one can measure $[O_3]$ simultaneously from the Hg absorption values prior to entering the flow cell, as well as by direct absorption of 308 nm in the flow cell under actual experimental conditions. The quantitative accuracy of this double calibration scheme is shown in Figure 3, which indicates a 1.02(4) ratio between the O_3 concentrations from flow rate

vs in situ absorption measurements. Although the two calibration methods agree to within experimental uncertainty, we consider the in situ measurement in the flow cell to be marginally more direct; thus, the O_3 concentrations in this work are either measured by laser absorption at 308 nm, or from the Hg lamp values modified by the calibration plot in Figure 3.

The IR single-mode laser source for the high-resolution infrared spectrometer is a modified color center laser, pumped by a Kr^+ laser (647.1 nm) and amplitude stabilized under servo loop control. Part of the color center output is used for a traveling Michelson interferometer[32] to read the absolute laser frequency and a scanning Fabry−Perot etalon (150 MHz) to provide frequency markers and to verify single mode operation. The radiation is split into signal and reference beam components, propagated though the photolysis cell or through an equivalent air path, and focused onto matched InSb detectors with <1 μs rise times. The color center laser output is collimated to 0.15 cm beam diameter (i.e., >7-fold smaller diameter than the UV photolysis beam) with a focusing lens/iris combination. The signal and reference detector outputs are subtracted in differential amplifiers optimized for high common mode rejection of laser amplitude noise, measured with a digital oscilloscope and transferred to a computer for storage and data analysis. The transient IR absorption signals are typically averaged over 500 excimer pulses to obtain signal to noise ratios of 100:1 or better. The time-resolved OH measurements are based on the P(2.5)1$^-$ transition[33] from the vibrational ground state at 3484.60 cm^{-1}. Transitions from other J states have been sampled to verify that collisional equilibration to a room temperature distribution is complete on the time scale of the chain reaction. The strong P(2.5)1$^-$ transition is chosen since the lower state is maximally populated at room temperature and not overlapped by any water absorption features in the flow cell.

III. Kinetic Analysis of Chain Reactions

As mentioned above, the chemical chain process is initiated by pulsed laser photolysis of O_3 at 308 nm in the red wing of the Hartley band, with an absorption cross section[2] of 13.4(5) $\times$ 10^{-20} cm^{-2} and an O(^{1}D) quantum yield[2] of approximately 75%

$$O_3 \rightarrow O_2 + O(^1D) \quad (75\%) \tag{4a}$$

$$O_3 \rightarrow O_2 + O(^3P) \quad (25\%) \tag{4b}$$

The excited O(^{1}D) atoms rapidly react with H_2O in the flow cell to yield both vibrationally "hot" (i.e., $v > 0$) and "cold" (i.e., $v = 0$) OH radicals[34,35]

$$O(^1D) + H_2O \rightarrow OH(\text{“hot”}) + OH(\text{“cold”}) \tag{5}$$

with a rate constant $k = 2.2 \times 10^{-10}$ cm^3 molecules^{-1} s^{-1}. There is also rapid competition to quench or react the O(^{1}D) species with O_3 ($k = 2.4 \times 10^{-10}$ cm^3 molecules^{-1} s^{-1}) or O_2 ($k = 3.2 \times 10^{-11}$ cm^3 molecules^{-1} s^{-1}) to yield ground state oxygen atoms or molecules via[36−38]

$$O(^1D) + O_3 \rightarrow O_2 + O_2 \tag{6a}$$

$$O(^1D) + O_3 \rightarrow O_2 + O(^3P) + O(^3P) \tag{6b}$$

$$O(^1D) + O_2 \rightarrow O_2 + O(^3P) \tag{7}$$

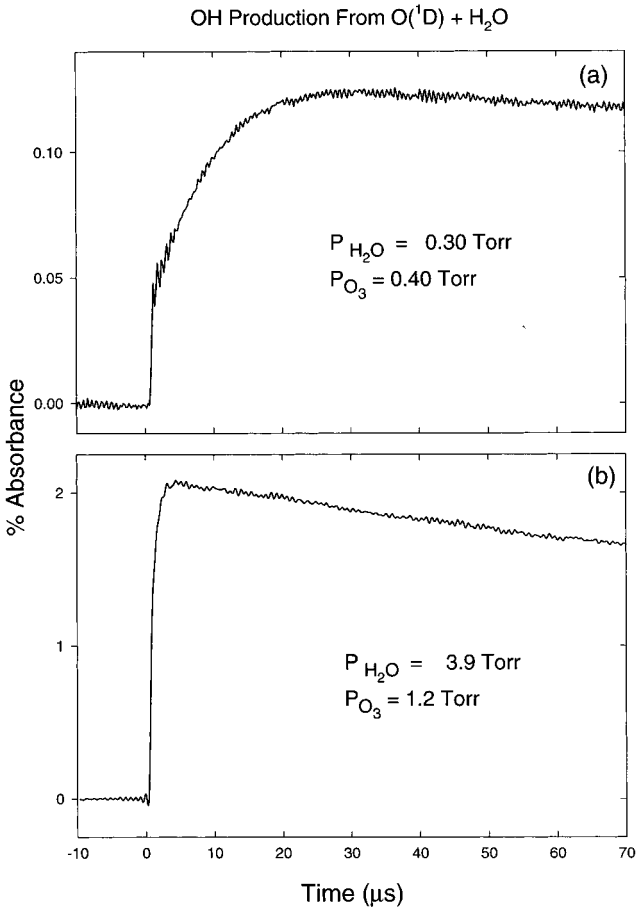

Figure 4. OH time profiles measured via time-resolved IR laser absorption on the $v = 1 \leftarrow 0$, P(2.5)1$^-$ transition. In a and b, the buffer gas conditions are chosen to modify the rate of collisional relaxation of the OH radicals, which in effect samples the early time scale dynamics for OH production. (a) At the lowest H_2O quenching gas concentrations, there is a "prompt" component of OH($v = 0$) absorption due to rapid reaction of O(^{1}D) with H_2O, which then rises to roughly twice this value with subsequent collisions in the buffer gas. This nearly 2-fold additional increase in OH signal reflects that vibrationally "hot" (i.e., $v > 0$) and "cold" OH($v = 0$) radicals are generated in roughly equal numbers, corresponding to "active" and "spectator" OH bonds in the O(^{1}D) + H_2O reaction. (b) For typical H_2O concentrations, however, this collisional relaxation is too rapid to distinguish these two components. The net effect is a prompt production of collisionally equilibrated OH radicals on the 5 μs time scale, which is much faster than the subsequent OH/HO_2/O_3 chain reaction kinetics of interest.

Since the high-resolution IR laser samples on P(2.5)1$^-$ transitions out of OH ($v = 0$, $J = 2.5$), the early time signals in Figure 4a reflect only the fraction of vibrationally "cold" OH radicals formed from reaction 5. Note that this early time component is followed by a slower, although still quite rapid exponential rise to nearly twice the initial value; this is due to rovibrational cooling of the "hot" OH species by collisions with H_2O and Ar buffer gas, which rapidly brings the system to room temperature equilibration. This approximate 2-fold increase in OH absorption amplitude is consistent with previous studies[34] of reaction 5, which indicate a nascent bimodal distribution of OH vibrationally hot and cold radical populations corresponding to "active" and "spectator" H atoms in H_2O, respectively. Under typical flow cell conditions, rapid quenching of these rovibrationally "hot" OH radicals [see Figure 4b], results in an essentially "prompt" rise in OH signals probed out of the $v = 0$, low N quantum levels, which on a much longer time scale reacts with O_3 to initiate the chemical chain reaction cycle. The key point is that the OH populations are equilibrated to a room

temperature distribution on <5 μs time scale, which is 1 or 2 orders of magnitude faster than the subsequent chain reaction kinetics under investigation.

Thus, for the purposes of kinetic analysis, initiation of the chain reaction can be approximated simply by prompt generation of $[OH]_0$ at $t = 0$. For typical XeCl pulse energies and beam sizes, $[OH]_0$ is 3 or 4 orders of magnitude smaller than $[O_3]$, which is necessary to ensure a pseudo-first-order kinetic regime and discriminate against radical−radical termination reactions. In this limit, the relevant coupled kinetic equations become

$$d[OH]/dt = -k_1[OH][O_3] + k_2[HO_2][O_3] \quad (8a)$$

$$d[HO_2]/dt = +k_1[OH][O_3] - k_2[HO_2][O_3] \quad (8b)$$

$$d[OH]/dt + d[HO_2]/dt = 0 \quad (8c)$$

where the last expression reflects the neglect of any net loss of chain radical concentration due to slow wall losses, diffusion, out of beam, etc. These kinetic equations can be readily solved for $[OH](t)$ and $[HO_2](t)$ to yield

$$[OH](t)/[OH]_0 = k_1/\{k_1 + k_2\} \exp\{-k_{ind}[O_3]t\} + k_2/\{k_1 + k_2\} \quad (9a)$$

$$[HO_2](t)/[OH]_0 = k_1/\{k_1 + k_2\} (1 - \exp\{-k_{ind}[O_3]t\}) \quad (9b)$$

where the effective chain induction rate and steady-state concentrations of OH radical and steady-state rate of chain propagation are given by

$$k_{ind} = \{k_1 + k_2\} \quad (10a)$$

$$[OH]_{ss} = [OH]_0 k_2/\{k_1 + k_2\} \quad (10b)$$

$$k_{prop} = \frac{k_1 k_2}{\{k_1 + k_2\}}[O_3] \quad (10c)$$

Equation 9a for the time dependence of [OH] illustrates several important points. First of all, $[OH](t)$ starts initially at $[OH]_0$ and undergoes single-exponential decay to a nonzero base line value of $[OH]_{ss} = [OH]_0 k_2/\{k_1 + k_2\}$ with a chain "induction" time constant $\tau_{ind} = \{k_{ind}[O_3]\}^{-1}$. This induction time constant reflects the time required for OH and HO_2 radicals to come into steady state, and therefore is controlled by the magnitude of *both* chain propagation steps. Consequently, any kinetic analysis of this exponential time dependence yields the *sum* of the two pseudo-first-order propagation rate constants. This is different from previous kinetic analyses[4,5,7] of OH + O_3 reaction rates, which neglect the slower second chain step and ascribe the observed time dependence entirely to $1/\tau_{ind} \approx k_1[O_3]$. Secondly, the OH decays to a *nonzero value* at $t \gg \tau_{ind}$ due to chain regeneration of OH from the secondary HO_2 + O_3 reaction. This also differs from previous analyses of OH + O_3 kinetics, which treat the OH signal as a *single* exponential decay down to $[OH]_{ss} \approx 0$ and ascribe this time constant to the first step in the chain reaction sequence.

Sample chain reaction data supporting this more complete kinetic analysis are presented in Figure 5, where the water and ozone reagent concentrations are listed in the figure caption. As predicted, the data unambiguously demonstrate single exponential decay from $[OH]_0$ to a *finite* $[OH]_{ss}$ plateau, which in turn decays on a much longer time scale ($t_{decay} \gtrsim 10$ ms) due to a combination of nonlinear chain termination and diffusion out of the probe laser IR beam volume. This point is

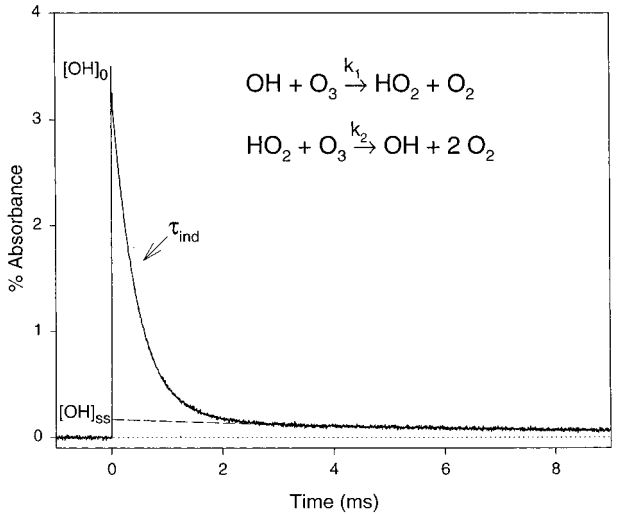

Figure 5. Typical time dependence of the OH absorption signal in the 10 ms time scale. The fast initial decay signals the "induction" of the chain reaction, followed by a much slower decay from the steady state "propagation" regime due to chain "termination" processes. The fast decay is determined by the *sum* of the two chain rate constants, whereas the ratio of fast- to slow-decay components reflects the *ratio* of the two chain rate constants. For this data, $[O_3] = 0.72$ Torr, $[H_2O] = 3.2$ Torr, [Ar] = 17.9 Torr, and the excimer photolysis intensity is 1.6 mJ/cm^2 per pulse. Under these experimental conditions, the number of chain cycles is $N_{chain} \approx 20$.

more dramatically made in logarithmic plots shown in Figure 6, which indicate a clear break characteristic of double-exponential decay behavior. Though this secondary decay is due to chain termination and therefore not predicted by the simple chain model, it can be easily treated by including *irreversible* (i.e., non-chain reaction sustaining) loss processes for OH and HO_2, as presented below.

Specifically, if we assume first-order, irreversible loss mechanisms for OH and HO_2 radicals, the relevant kinetic equations are modified to become

$$d[OH]/dt = -k_1[OH][O_3] + k_2[HO_2][O_3] - k_{irr}^{OH}[OH] \quad (11a)$$

$$d[HO_2]/dt = +k_1[OH][O_3] - k_2[HO_2][O_3] - k_{irr}^{HO_2}[HO_2] \quad (11b)$$

$$d[OH]/dt + d[HO_2]/dt = -k_{irr}^{OH}[OH] - k_{irr}^{HO_2}[HO_2] \quad (11c)$$

Efficient propagation occurs when irreversible loss of OH and HO_2 is *slow*, and thus the chain reaction is sustained for many cycles. This is kinetically equivalent to saying that the OH/HO_2 ratio is maintained in a steady-state ratio k_2/k_1, even as both chain radical species are eventually consumed irreversibly. In this simplifying limit of k_{irr}^{OH}, $k_{irr}^{HO_2} \ll k_{ind}$, eq 11a−c can be solved to yield

$$[OH](t)/[OH]_0 \approx k_1/\{k_1 + k_2\} \exp\{-k_{ind}[O_3]t\} + k_2/\{k_1 + k_2\} \exp\{-k_{term}t\} \quad (12)$$

This now correctly predicts a *double*-exponential decay in the OH signal, with the faster chain induction component given by k_{ind} and a slower chain *termination* component given by

$$k_{term} = k_{irr}^{OH} k_2/\{k_1 + k_2\} + k_{irr}^{HO_2} k_1/\{k_1 + k_2\} \quad (13)$$

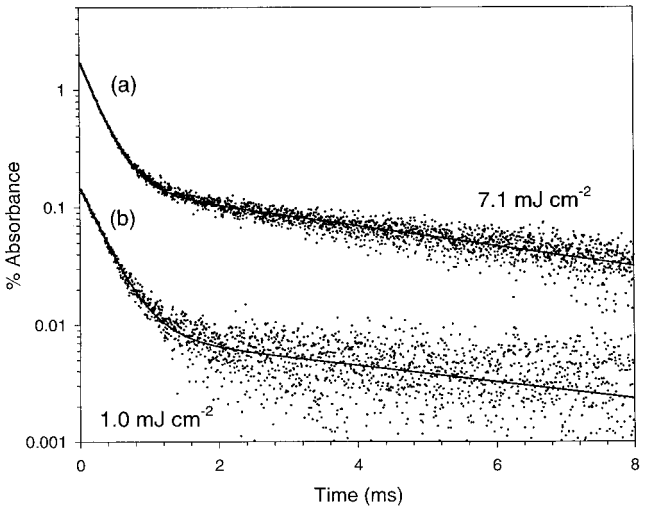

Figure 6. Logarithmic plot of the absorbance depending on time for (a) 7.1 mJ/cm^2 and (b) 1.0 mJ/cm^2 UV laser intensities. For this comparison, the experimental concentrations are held constant at [O_3] = 1.1 Torr, [H_2O] = 4.1 Torr, and [Ar] = 19.5 Torr. Note the clear break in slopes characteristic of double-exponential decay and the lack of sensitivity to [OH] radical concentration.

It is interesting to note from eq 13 that the chain termination rate reflects a *sum of both* OH and HO_2 loss rates, but now weighted by the fractional steady-state concentrations of each radical. As a result, these OH/HO_2/O_3 chains can still propagate quite efficiently even in the presence of relatively fast irreversible removal processes for OH, due simply to the fact that the *overall* concentration of chain radicals (i.e., [OH] + [HO_2]) is "stored" as the less reactive HO_2 radical. Note also that this model predicts the *ratio* of k_1/k_2 to be determined by the relative amplitudes of the fast- and slow-decay components back extrapolated to $t = 0$. Finally, the total number of chain cycles is typically dominated by the long time propagation behavior, which can be found by integration of eq 12 to yield

$$N_{\text{cycles}} \approx k_{\text{prop}}/k_{\text{term}} = k_1k_2[O_3]/\{k_{\text{irr}}^{\text{OH}}\, k_2 + k_{\text{irr}}^{\text{HO}_2}\, k_1\} \qquad (14)$$

In summary, the above kinetic analysis makes three predictions. (1) In the limit of efficient chain propagation and slow chain termination processes, double-exponential time dependence of the OH chain radicals is anticipated. (2) A plot of the fast decay rate vs [O_3] will yield a slope of $\{k_1 + k_2\}$ (i.e., the *sum* of the two chain propagation reaction rate constants). (3) The ratio of back extrapolated components for fast (induction) and slow (termination) decays yields k_1/k_2 (i.e., the ratio of the two chain propagation rate constants).

IV. Results and Discussion

To obtain the desired kinetic rate information, time-resolved IR absorption traces for loss of OH radical after excimer laser initiation are obtained for a wide variety of experimental conditions. To verify that the kinetic results are quantitatively reliable, these experiments have been exhaustively repeated for ≈140 different cell pressures, buffer gases, flow rates, photolysis energies, and over a 1000-fold dynamic range of ozone concentrations. An abbreviated list of the experimental conditions is summarized in Table 2. A more complete discussion of these various experimental checks is deferred until later in this section. Each OH radical time trace is then fitted to the double exponential decay form predicted in eq 12 using nonlinear least-squares routines to extract k_{ind}, k_{term} and the ratio of the fast- and slow-decay components. Sample-fitted data are shown in Figure 5, which indicate the high signal-to-noise (S/N) quality and small residuals obtained from the least-squares-fitting procedure. From eq 14, these experimental conditions support over 20 complete chain cycles (i.e., more than 40 molecules of O_3 are destroyed for each OH radical generated photolytically). The chain induction rate component (k_{ind}) has been plotted vs ozone concentration in Figure 7. From a linear least-square analysis, the slope of this fit (i.e., the induction rate constant) at 298 K is $k_{\text{ind}} = k_1 + k_2 = 8.4(8) \times 10^{-14}$ cm^3 molecule^{-1} s^{-1}, with an intercept which is negligible within uncertainty. It is worth stressing that these data reflect the results of ≈140 separate kinetic measurements, taken at over

TABLE 2: Summary of Experimental Conditions

no. of data runs	laser energy (mJ cm^{-2} pulse^{-1})	H_2O pressure (Torr)	total pressure[a] (Torr)	[O_3][b] × 10^{16} molecules/cm^3	k_{ind}[c] (10^{-14} cm^3 s^{-1})
19	7.5	5.0	45.0	0.097−9.46	8.2(8)
21	4.3	6.6	34.9	0.25−7.56	8.7(8)
6	5.0	5.3	29.7	0.13−1.16	9.2(9)
21	4.9	4.0	24.6	0.20−6.45	8.3(8)
21	2.8	1.3	42.5	0.47−7.62	9.1(9)
20	1.6	3.3	23.4	0.42−6.69	8.7(8)
12	2.4	6.0	16.7	0.50−4.59	11.0(11)
19	2.6	12.5	43.4	0.095−4.52	8.0(8)

[a] Typically with Ar buffer gas, though additional tests have been performed with SF_6, N_2, and O_2 buffer gas. [b] Range of [O_3] sampled at the stated laser energy, [H_2O] and total cell pressure. [c] k_{ind} values obtained from analysis of each data subset; the reported value of $k_1 + k_2 = 8.4(8) \times 10^{-14}$ cm^3 molecule^{-1} s^{-1} represents a least-squares fit to the combined data set, as shown in Figure 7.

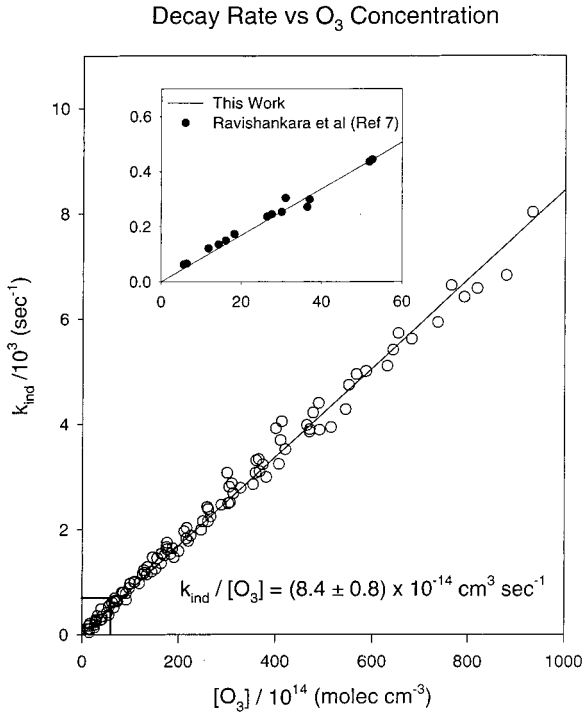

Figure 7. Stern−Volmer analysis of decay time vs ozone concentration at 298 K for various different experimental conditions. The slope represents the sum of the two chain rate constants, $k_{\text{ind}} = k_1 + k_2 = 8.4(8) \times 10^{-14}$ cm^3 molecule^{-1} s^{-1}. This data reflects ≈140 different sets of independent experimental conditions taken over several months, covering (i) a 5-fold range of excimer laser intensities (1.6−7.5 mJ/cm^2), (ii) a 10-fold range of [H_2O] (1.3−12.5 Torr), (iii) a 3-fold range of total cell pressure (16.7−45.0 Torr), and (iv) a 1000-fold range of [O_3] (9.7×10^{14} and 9.5×1016 molecules/cm^3). The explicit ranges of conditions for separate data runs are summarized in Table 2.

a 50-fold dynamic range in laser pulse energies and cell pressures, as well as over a 100-fold dynamic range in $[O_3]$.

Though such chain reaction kinetics have been present in previous experimental studies, the effects require relatively high S/N to see unambiguously. Furthermore, detection of the steady state chain regime is enhanced by the higher ozone concentrations accessible to the present IR method, which is able to make the initial decay rapid with respect to radical−radical chain termination processes and diffusion out of the probe beam. This is the first kinetic study of the $O_3/OH/HO_2$ reaction system that takes chain propagation effects explicitly into account, and which therefore reports the *sum* of the two chain rate constants (i.e., $k_{ind} = k_1 + k_2$). By way of contrast, previous kinetic analyses have approximated the loss of OH as a single-exponential function of time and report a value for k_1 alone. From section 3, it is clear that this is not rigorously correct; for the $OH/HO_2/O_3$ chain reaction system, however, the magnitude of k_2 is thought to be only <5% of k_1, which explains why the second decay component would only be evident at high S/N in the previous studies. In the current studies, this double-exponential behavior is evident in all kinetic traces and is explicitly included in the kinetic analyses. Thus for consistency, the present results for k_{ind} should be compared with the earlier values reported for k_1 from previous studies that presumed a purely single-exponential decay.

These results are in agreement with the previous room temperature RF studies of Ravishankara et al.,[7] who report a rate constant of 8.2×10^{-14} cm^3 molecule^{-1} s^{-1}. To make this more explicit, we have replotted the Ravishankara et al. data[7] on top of the current data (see inset region in Figure 7), which indicates a nearly quantitative overlap but also underscores the ≈10−20 fold *larger* range of ozone concentrations that have been investigated via the IR laser absorption method. As indicated in Table 1, there is a relatively broad range of rate values reported in the literature;[4−7] our data is most consistent with the Ravishankara et al. value,[7] verified over a much larger dynamic range of $[O_3]$. Of particular importance, the presently determined value for k_{ind} is >20% higher than obtained from the k_1 and k_2 values recommended for use in atmospheric modeling.[1]

As additional confirmation of these results, the measurements have been repeated under a variety of diagnostic test conditions. The first is to assess for any effects due to nonlinear radical−radical kinetics, which one can systematically check by varying the laser power. The lack of any dependence on excimer laser power is displayed in Figures 6 and 8a, which indicate no change in the reported value of k_{ind} over a factor of 50 in laser pulse energy. For comparison, most of the experiments reported in Figure 7 are conducted with laser energy of about ≲1 mJ/ cm^2 at a typical ozone concentration of 10^{16} molecules/cm.[3] This corresponds to an initial OH radical concentration of ≈10^{12} molecules/cm^3 and a $[OH]_0/[O_3]$ ratio of ≈10^{-4}. This low ratio of radical to O_3 concentrations ensures first-order kinetics and discriminates against contributions from even gas kinetic radical−radical reactions such as $OH + HO_2$ on the time scale of chain reaction induction period.

A second issue to address is the degree of thermal equilibration of the OH radical. As noted by Ravishankara et al.,[7] this can be particularly important in the $OH/HO_2/O_3$ chain reaction system due to acceleration of the $OH + O_3$ chain step by OH vibrational excitation.[39] To eliminate these interferences, the flow cell mixture contains high concentrations of H_2O, which

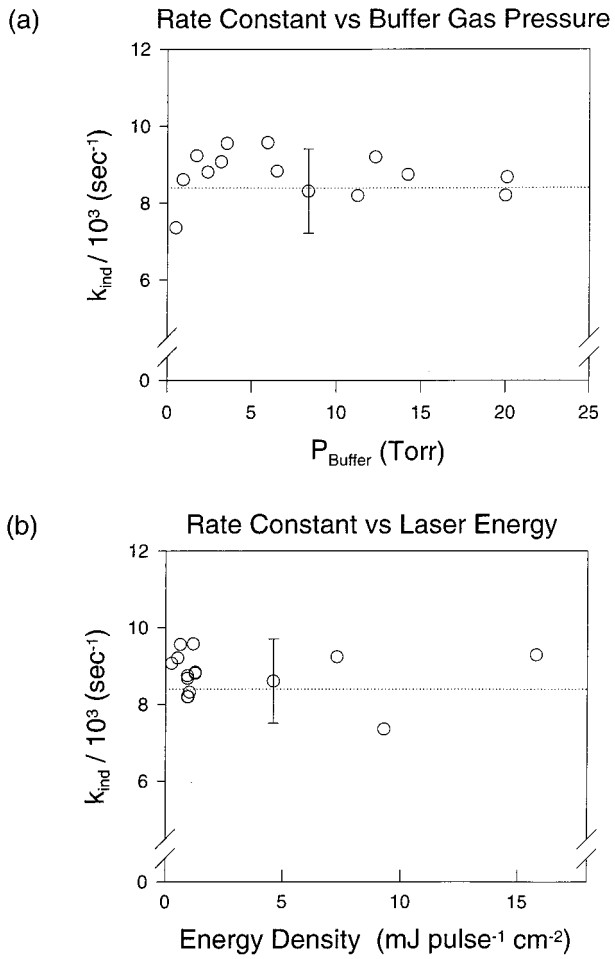

Figure 8. Further confirmational tests of the kinetic analysis, demonstrating independence on (a) the excimer photolysis energy density and (b) buffer gas concentration.

is an extremely efficient quencher of vibrationally as well as rotationally excited OH radical. This can be tested in several ways. First of all, this degree of internal state relaxation is confirmed in Figure 4b, which indicates the excellent temporal separation between fast OH rovibrational relaxation and the much slower removal of OH by chain reaction with O_3. Secondly, since the IR probe laser is quantum state specific, we can monitor the chain kinetics on different rotational levels, which indicate no difference within experimental uncertainty. Furthermore, these kinetic measurements have been repeated for a variety of buffer gases (Ar, SF_6, N_2, and O_2) and cell pressures. As displayed in Figure 8a,b the observed rates are remarkably insensitive to buffer gas conditions over the full range of data represented in Figure 7.

As a final note, the chain kinetic analysis presented in section 3 predicts that the ratio of k_2/k_1 can be obtained from the ratio of back extrapolated amplitudes for the slow- and fast-decay components. Indeed, from an average over all the data represented in Figure 7, this ratio is found to be $k_2/k_1 \approx 0.05$-(3), although there is currently an appreciable level of scatter in these results. This is at least consistent with the previous measurements of k_2 by Zahniser and Howard,[6] which yield $k_2/k_1 \approx 0.026(3)$, as well as their LMR measurements of $[HO_2]_{ss}/[OH]_{ss} \approx 35(8)$ in the steady state regime, which would predict $k_2/k_1 \approx 0.028(7)$. From preliminary results at 193 nm, this scatter in the ratio of fast- and slow-decay components appears to be due to initial O(^{3}P) concentration in the flow cell. This O(^{3}P) concentration arises from (i) finite O(^{1}D) quantum yield

from photolysis of O_3, as well as (ii) non reactive quenching of $O(^1D)$ with O_3 or H_2O, which currently limits a more quantitative extraction of k_2/k_1. Specifically, on the much longer time scales of chain propagation and termination, $O(^3P)$ atoms can act as an alternate pathway for "recycling" HO_2 chain radicals back to OH by the fast reaction

$$O(^3P) + HO_2 \rightarrow OH + O_2 \qquad (15)$$

which occurs with a rate constant[40] at room temperature of 5.9×10^{-11} cm^3 molecule^{-1} s^{-1}. This is at first somewhat surprising, since reaction 15 represents a radical−radical loss mechanism that should be negligible at sufficiently low radical densities. However, although $[O(^3P)]$ is typically $\approx 10^5$ times *smaller* than $[O_3]$, the corresponding reaction rate with HO_2 radical is nearly gas kinetic and $\approx 3 \times 10^4$ faster than the $HO_2 + O_3$ reaction. Thus, even for the relatively low radical densities in the flow cell, reaction 15 can still be contributing to net regeneration of OH chain radicals from HO_2, and thereby influence the back-extrapolated ratio of $[OH]_{ss}/[OH]_0$. These expectations have been explicitly tested by numerical integration of coupled kinetic equations including radical−radical reactions of $O(^3P)$, OH, and HO_2, as well as reactions with and quenching of $O_2(^1\Delta)$ formed from the initial photolysis of ozone. Such simulations confirm that the fast "induction" analysis of $k_1 + k_2$ is not influenced significantly, but that these nonlinear radical−radical processes can perturb the inferred $[OH]_{ss}/[OH]_0$ ratios by an amount consistent with the observed scatter. Thus, rate constant measurements for the slow step of the chain will necessitate further kinetic studies with $[O(^3P)]/[O_3]$ ratios reduced to even lower (i.e., a few ppm) levels.

V. Summary

A new experimental method for kinetic study of ozone chemical chain reactions is presented based on the combination of excimer laser photolysis and detection of OH radical by time-resolved absorption of high-resolution IR laser light. This IR based method is particularly advantageous for application to the $OH/HO_2/O_3$ chain reaction system, due to the complete lack of O_3 absorption in the OH stretch region. As a result, the chain kinetics can be studied over a much larger dynamic range of O_3 concentrations than previously accessible via laser induced fluorescence or resonance fluorescence methods for monitoring time dependent OH radical concentrations. The access to higher O_3 concentrations allows the chain reaction kinetics of (i) induction, (ii) propagation, and (iii) termination steps to be cleanly separated in time.

A pseudo-first-order kinetic analysis is presented which correctly predicts the OH time dependence to be double exponential, with an initial exponential component determined by the *sum* of the two chain rate constants (i.e., $k_{ind} = k_1 + k_2$). Furthermore, this chain "induction" feature decays to a nonzero OH concentration in the steady-state chain propagation regime, which is also confirmed by experimental results. This analysis differs from previous LIF/RF studies of $OH + O_3$, which neglect chain effects due to the $HO_2 + O_3$ reaction and treat the loss of OH as a single-exponential decay to zero determined only by k_1. Our data analysis yields a value for the $k_{ind} = k_1 + k_2 = 8.4(8) \times 10^{-14}$ cm^3 molecule^{-1} s^{-1}, which is confirmed over a much higher dynamic range of ozone concentrations than previously accessible by LIF and RF methods. These results are quantitatively consistent with the previous rate constant values of Ravishankara et al., but are substantially higher than the values currently recommended for use in atmospheric modeling. Further work is currently underway to determine the temperature dependence of these chain rates down to temperatures ($\lesssim$200 K) relevant to atmospheric modeling.

Acknowledgment. Support for this work was provided by National Aeronautics and Space Administration and the Air Force Office of Scientific Research. A.K. thanks the Deutsche Forschungsgemeinschaft for a research fellowship. Finally, the authors acknowledge numerous valuable discussions with C. J. Howard, A. R. Ravishankara, and A. J. Langford, as well as thank C. J. Howard for a generous loan of the ozone flow calibration apparatus.

References and Notes

(1) DeMore, W. B.; Sander, S. P.; Golden, D. M.; Hampson, R. F.; Kurylo, M. J.; Howard, C. J.; Ravishankara, A. R.; Kolb, C. E.; Molina, M. J. Chemical Kinetics and Photochemical Data for Use in Stratospheric Modeling. Technical Report 94-26; NASA/JPL: Houston, 1994.
(2) Brasseur, G.; Solomon, S. *Aeronomy of the Middle Atmosphere*; Reidel: Dordrecht, 1986.
(3) World Meteorological Organization; *Scientific Assessment of Ozone Depletion: 1994*; Organization: Geneva, 1995.
(4) Anderson, J. G.; Kaufman, F. *Chem. Phys. Lett.* **1973**, *19*, 483.
(5) Kurylo, M. J. *Chem. Phys. Lett.* **1973**, *23*, 467.
(6) Zahniser, M. S.; Howard, C. J. *J. Chem. Phys.* **1980**, *73*, 1620.
(7) Ravishankara, A. R.; Wine, P. H.; Langford, A. O. *J. Chem. Phys.* **1979**, *70*, 984.
(8) Smith, C. A.; Molina, L. T.;. Lamb, J. J; Molina, M. J. *Int. J. Chem. Kin.* **1984**, *16*, 41.
(9) Sinha, A.; Lovejoy, E. R.; Howard, C. J. *J. Chem. Phys.* **1987**, *87*, 2122.
(10) Simonaitis, R.; Heiklen, J. *J. Phys. Chem.* **1973**, *77*, 1932.
(11) DeMore, W. B.; Tschuikow-Roux, E. *J. Phys. Chem.* **1974**, *78*, 1447.
(12) DeMore, W. B. *J. Phys. Chem.* **1979**, *83*, 1113.
(13) Cox, R. A.; Hayman, G. D. *Nature* **1988**, *332*, 796.
(14) Anderson, J. G.; Brune, W. H.; Proffitt, M. J. *J. Geophys. Res.* **1989**, *94*, 11.
(15) Molina, L. T.; Molina, M. J. *J. Chem. Phys.* **1987**, *91*, 433.
(16) Molina, M. J.; Bo, T.-L.; Molina, L. T.; Yang, F. C. Y. *Science* **1988**, *238*, 1253.
(17) Hunt, B. G. *J. Geophys. Res.* **1966**, *71*, 1385.
(18) Whitten, R. C.; Borucki, W. J.; Capone, L. A.; Turco, R. P. *Nature* **1978**, *275*, 523.
(19) Crutzen, P. J.; Howard, C. J. *Pure Appl. Geophys.* **1978**, *116*, 497.
(20) Duewer, W. H.; Wuebbles, D. J.; Ellsaesser, H. W.; Chang, J. S. *J. Geophys. Res.* **1977**, *82*, 935.
(21) Nesbitt, D. J.; Leone, S. R. *J. Chem. Phys.* **1980**, *72*, 1722.
(22) Nesbitt, D. J.; Leone, S. R. *J. Chem. Phys.* **1981**, *75*, 4949.
(23) Dolson, D. A.; Leone, S. R. *J. Chem. Phys.* **1982**, *77*, 4009.
(24) Schiffman, A.; Nelson, D. D., Jr.; Robinson, M.; Nesbitt, D. J. *J. Phys. Chem.* **1991**, *95*, 2629.
(25) Schiffman, A.; Nesbitt, D. J. *J. Chem. Phys.* **1994**, *100*, 2677.
(26) German, K. R. *J. Chem. Phys.* **1975**, *63*, 5252.
(27) Coleman, E.; Siegrist, T.; Mixon, D. A.; Trevor, P. L.; Trevor, D. J. *J. Vac. Sci. Technol.* **1991**, *A9*, 2408.
(28) Cook, G. A.; Kiffer, A. D.; Klumpp, C. V.; Malik, A. H.; Spence, L. A. *Ozone Chemistry and Technology*; American Chemical Society: Washington, DC, 1959.
(29) Hearn, A. G. *Proc. Phys. Soc., London* **1961**, *78*, 932. Mauersberger, K. J.; Hanson, D.; Morton, J. *Geophys. Res. Lett.* **1986**, *13*, 671.
(30) Mount, G. *J. Geophys. Res.* **1992**, *97*, 2427.
(31) Bass, A. M.; Paur, R. J. *Proceedings of the Quadrientennial Ozone Symposium*; Reidel: Hingham, MA, 1984; p 606.
(32) Hall, J. L.; Lee, S. A. *Appl. Phys. Lett.* **1976**, *29*, 367.
(33) Coxon, J. A. *Can. J. Phys.* **1980**, *58*, 933.
(34) Butler, J. E.; Talley, L. D.; Smith, G. K.; Lin, M. C. *J. Chem. Phys.* **1981**, *74*, 4501.
(35) Davidson, J. A.; Schiff, H. I.; Brown, T. J.; Howard, C. J. *J. Chem. Phys.* **1978**, *69*, 4277; Wine, P. H.; Ravishankara, A. R. *Chem. Phys.* **1982**, *69*, 365.
(36) Streit, G. E.; Howard, C. J.; Schmeltekopf, A. L.; Davidson, J. A.; Schiff, H. I. *J. Chem. Phys.* **1976**, *65*, 4761.
(37) Lee, L. C.; Slanger, T. G. *J. Chem. Phys.* **1978**, *69*, 4053.
(38) Davenport, J. E.; Ridley, B.; Schiff, H. I.; Welge, K. H. *J. Chem. Soc. Faraday Disc.* **1972**, *53*, 230.
(39) Streit, G. E.; Johnston, H. S. *J. Chem. Phys.* **1976**, *64*, 95.
(40) Ravishankara, A. R.; Wine, P. H.; Nicovich, J. M. *J. Chem. Phys.* **1983**, *78*, 6629.